Geological Magazine

www.cambridge.org/geo

Discussion - Reply

Cite this article: Kumar A, Dutt S, Saraswat R, Gupta AK, Clift PD, Pandey DK, Yu Z, and Kulhanek DK (2020) Late Pleistocene sedimentation in the Indus Fan, Arabian Sea, IODP Site U1457. *Geological Magazine* **157**: 920–928. https://doi.org/10.1017/S0016756819000396

Received: 30 August 2018
Revised: 19 March 2019
Accepted: 2 April 2019
First published online: 17 May 2019

Keywords:
Laxmi Basin; Indus Fan; Arabian Sea; grain-size distribution; IODP

Author for correspondence: Anil Kumar, Email: akumar@wihg.res.in

Late Pleistocene sedimentation in the Indus Fan, Arabian Sea, IODP Site U1457

Anil Kumar[1], Som Dutt[1], Rajeev Saraswat[2], Anil Kumar Gupta[3], Peter D Clift[4], Dhananjai Kumar Pandey[5], Zhaojie Yu[6] and Denise K Kulhanek[7]

[1]Wadia Institute of Himalayan Geology, 33 GMS Road, Dehradun, India; [2]Geological Oceanography Division, National Institute of Oceanography, Goa, India; [3]Department of Geology and Geophysics, Indian Institute of Technology Kharagpur, Kharagpur, W.B. 721302, India; [4]Department of Geology and Geophysics, Louisiana State University, Baton Rouge, LA 70803, USA; [5]ESSO – National Centre for Antarctic and Ocean Research, Goa, India; [6]Université de Paris-Sud, Orsay, France and [7]Texas A&M University, 1000 Discovery Drive, College Station, TX 77845, USA

Abstract

The intensity of turbidite sedimentation over long timescales is driven by sea-level change, tectonically driven rock uplift and climatically modulated sediment delivery rates. This study focuses on understanding the effect of sea-level fluctuations and climatic variability on grain-size variations. The grain size and environmental magnetic parameters of Arabian Sea sediments have been documented using 203 samples, spanning the last 200 ka, obtained from International Ocean Discovery Program (IODP) Site U1457. Grain-size end-member modelling suggests that between ~200 and 130 ka there was an increase in the coarse silt fraction caused by sediment transport following reworking of the Indus Fan and development of deep-sea canyons. The sediment size and enhanced magnetic susceptibility indicate a dominant flux of terrestrial sediments. Sedimentation in the distal Indus Fan at *c.* 200–130 ka was driven by a drop in sea level that lowered the base level in the Indus and Narmada river systems. The low sea-stand caused incision in the Indus delta, canyons and fan area, which resulted in the transportation of coarser sediment at the drilling site. Magnetic susceptibility and other associated magnetic parameters suggest a large fraction of the sediment was supplied by the Narmada River during ~200–130 ka. Since ~130 ka, clay-dominated sedimentation is attributed to the rise in sea level due to warm and wet climate.

1. Introduction

The Ganga–Brahmaputra and Indus rivers carry huge volumes of sediment from the Himalaya to the foreland and finally to the deep ocean. The resultant marine sediments record the prevailing climatic and tectonic signals, with foreland basins representing largely transient depocentres (Goodbred, 2003). The Indus River, like the Ganga–Brahmaputra river system, has a dispersal mechanism that carries sediments from the western Himalaya and Karakoram to the Indus Delta (Clift & Giosan, 2014) that are subsequently deposited in a submarine fan. The growth of the submarine fan depends on the sediment flux from the continent via fluvial and, to a much lesser extent, aeolian transport. Erosion in the Indus basin is controlled by glaciation and precipitation caused by both mid-latitude westerlies and the southwest monsoon, with rock uplift in the source regions playing a role over longer timescales (Burbank *et al.* 1996; Clift & Giosan, 2014; Munack *et al.* 2014; Kumar & Srivastava, 2017). In order to extract climatic and tectonic signals from the sediment record, an understanding of lag times between erosion, transport and final sedimentation is crucial. The path length from sediment generation to the deposition partly controls the lag time, with longer transient zones in the sediment routing system often resulting in greater mass storage and longer lag times (Romans *et al.* 2016). The propagation of climate and/or tectonic perturbations through sediment transportation from source to sink depends upon how the landscape responds to such forcing processes (Fildani *et al.* 2016). For example, the Mississippi river system responded to the glacial–eustatic low-stand by transferring an enormous sediment mass to the Mississippi Fan (Filadani *et al.* 2016). Leads and lags in signal propagation can be tackled through estimation of the timing and magnitude of mass storage in the transient zone (Romans *et al.* 2016).

Sandy materials are estimated to take 5–10 ka to reach the shoreline and possibly as long as 100 ka to reach the submarine fan (Clift & Giosan, 2014; Li *et al.*, 2018). Post-depositional processes such as contour currents can also affect sedimentation. Turbidity current sedimentation, responsible for much of the sediment transport to the deep water fan, over timescales of 10^3 –10^6 years, is controlled by sea-level fluctuations and sediment supply itself driven by climate variability and tectonic forces. Turbidite frequency and rates of sedimentation in the Arabian Sea are controlled by changes in sea level during the Quaternary period (Prins & Postma, 2000; Ferrier *et al.*, 2015). Sea-level changes typically affect sedimentation over astronomical

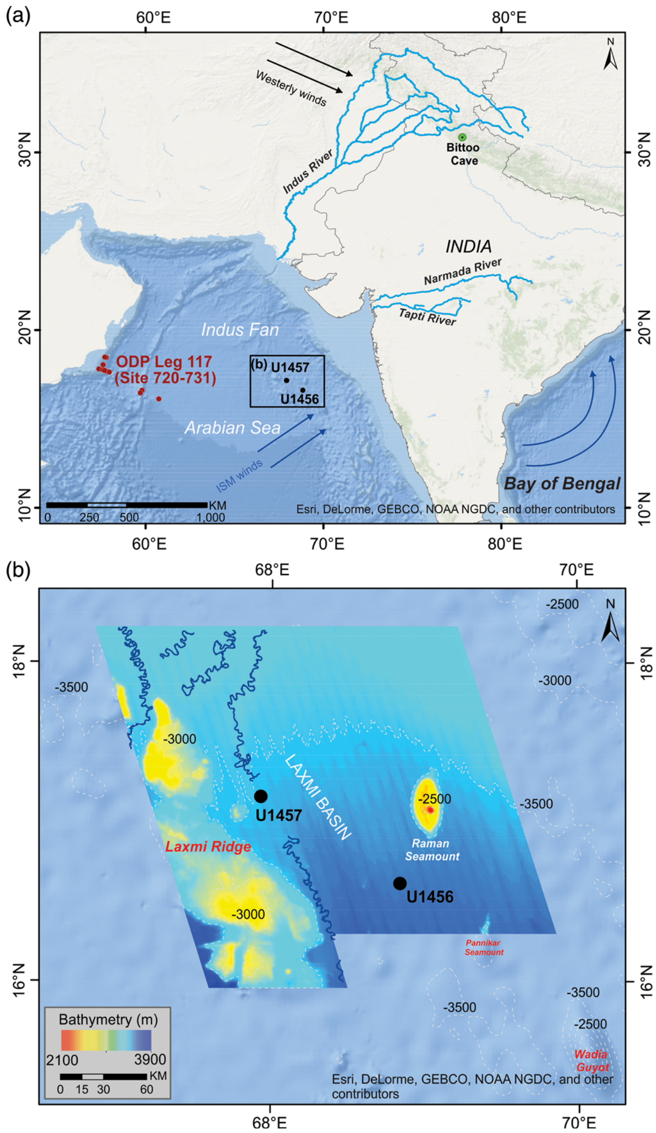

Fig. 1. (a) Map showing location of the IODP Sites U1456 and U1457 in the eastern Arabian Sea overlain on a regional bathymetric map. Course of the major river systems draining to the Arabian Sea is also displayed. (b) An enhanced bathymetric grid (after Prerna *et al*. 2015) of the rectangular block shown in (a) with a number of active channels surrounding drill sites.

timescales (21–100 ka), since the onset of the Northern Hemisphere glaciation (Cazenave & Llovel, 2010), although there is a tectonic control on longer timescales. On longer timescales (10^6 years), deep-water sedimentation is driven by sediment flux caused by erosion of tectonically uplifting bedrock sources modulated by long-term evolution of the Indian summer monsoon (ISM) (Mitrovica *et al.* 2001; Mitrovica & Milne, 2002; Clift *et al.* 2008). Deep-water sedimentation is also affected by the stream/river flow intensity during transport from continents to the adjacent ocean basin (Ivins *et al.* 2007; Simms *et al.* 2007, 2013; Blum *et al.* 2008; Wolstencroft *et al.* 2014). Sedimentation in submarine fans, such as the Amazon, Mississippi and Bengal fans, records the landscape evolution of continents, ice retreat events in glacial–interglacial times, catchment widening via erosion and climatic fluctuation (Flood *et al.* 1991; Kolla & Perlmutter, 1993; Weber *et al.* 1997; Goodbred, 2003; Fildani *et al.* 2016, 2018). Deep-sea turbidity currents modify the sea bottom by building up vertical and horizontal stratigraphy through channel levee deposits. These channel levee deposits are characteristic trails of sediment transport across the deep basin floor (Kolla, 2007). Sediments in the Arabian Sea can capture signals of ISM variability over centennial to million-year timescales in hemipelagic sedimentation and turbidites (Clemens & Prell, 1990; Clemens *et al.* 1991; Prins & Postma, 2000; Gupta *et al.* 2003, 2015; Saraswat *et al.* 2005; Ziegler *et al.* 2010; Tripathi *et al.* 2017). Despite the strong climatic forcing, long and continuous records of erosional sedimentation based on deposits in foreland basins remain elusive (Najman, 2006). Therefore, retrieving precise records of climate–tectonic–erosion interactions over shorter timescales from the proximal ocean basins is essential. Furthermore, such records enable constraint of lead and lag times between weathering/erosion and final sedimentation. This relationship is largely unexplored for the Indus Fan in the Arabian Sea. In this study, we have characterized sediments from the eastern Arabian Sea to understand the role of sea-level fluctuations and climatic variability in controlling sediment flux to the deep ocean.

2. Drilling sites

IODP Site U1457 (17° 9.95′ N, 67° 55.80′ E), cored during IODP Expedition 355, is located in the Laxmi Basin, ~490 km west of the Indian coast and in 3534 m water depth in the eastern Arabian Sea (Fig. 1; Pandey *et al.* 2016). The Laxmi Basin is a shelf-parallel marginal basin adjacent to the western continental margin of India. The origin of the basin is linked to late Cretaceous continental break-up of the Indian Ocean (Royer *et al.* 2002; Pandey & Pandey, 2015). The Laxmi Ridge separates the Laxmi Basin from the main basin of the Arabian Sea. The drilling site was chosen after seismic surveying and regional correlation with industrial borehole data on the Indian shelf. The seismic characteristics and bathymetric survey suggested a muddy and undisturbed seafloor (Pandey *et al.* 2015). Since its inception, the Laxmi Basin has received sediments from the Indus River, as well as from peninsular Indian rivers (i.e. Narmada and Tapti rivers), although their discharge is much less than that of the Indus River. The present-day sediment loads of the Narmada and Indus rivers are ~35×10^6 and ~250×10^6 ton a^{-1}, respectively (Milliman & Syvitski, 1992; Gupta & Chakrapani, 2005). This study involves 203 sediment samples from IODP Site U1457 taken from depths down to 10.5 m below seafloor (mbsf) at a 7 cm resolution.

3. Materials and methods

3.a. Grain-size characterization and end-member analysis

Grain-size data combined with end-member analysis of sediment facilitate understanding of the depositional setting, energy conditions and sediment transport mechanisms. Both the raw grain-size analysis of marine sediments and their end-member analysis help in understanding the energy of the transporting medium (Weltje & Prins, 2003; Prizomwala *et al.* 2014). The grain size of 203 samples was measured using a Laser Particle Size Analyzer (LPSA) (Malvern Mastersizer MU 2000) at the Wadia Institute of Himalayan Geology, Dehradun, following the procedure described in Dutt *et al.* (2018). Before analysis, all the samples were treated with 10 % HCl, followed by 40 % H_2O_2 for removing carbonates and organic material, respectively. HCl and H_2O_2 were removed after treatment by using distilled water and centrifuging three times for 3 min each time at 6000 rpm. Prior to measurement,

https://doi.org/10.1017/S0016756819000396 Published online by Cambridge University Press

samples were disaggregated in distilled water, with a 2300 rpm stirrer and 40 % ultrasonic vibrator for 45 s. Five measurements were taken for each sample in order to ensure the best results. The average of all five measurements was used for further interpretation. These grain-size data were then processed, and meaningful end-members were identified using the method of Weltje & Prins (2007). This was done to understand different transportation processes and constrain the related sediment flux. The end-member modelling analysis (EMMA) was done by implementing the EMMAgeo version 0.9.2 package in R language (by M Dietze & E Dietze, 2015. In comparison to other statistical methods, e.g. moment method, EMMA is a statistical tool used for unmixing the mixed dataset and generates end-members which explain the maximum variance of the data (Weltje & Prins, 2007). Grain sizes were classified based on the Udden–Wentworth grade scale (Udden, 1914; Wentworth, 1922). The statistical parameters were calculated using the graphical moment method. The EMMA was applied to the grain-size data to understand the hydrological energy conditions active during deposition (Weltje & Prins, 2007). In general, we associate larger grain size with higher-energy sedimentation, which might indicate increased sediment flux from the continent, lower sea-level or simply the avulsion of the depositional lobes on the submarine fan from one location to another.

3.b. Environmental magnetism

Environmental magnetic parameters of sediments are widely used to characterize the magnetic minerals present and their concentration. In different depositional settings, these parameters provide information about the regional palaeo-environmental conditions, post-depositional alteration and sediment source (Bloemendal *et al.* 1993; Evans & Heller, 2003; Kumar *et al.* 2017). Environmental magnetic parameters were measured on 134 sediment samples from Site U1457. A fraction of well-mixed sediment was packed into 10 cm^3 non-magnetic styrene vessels. Magnetic susceptibility was measured at low and high frequencies (0.47 and 4.7 kHz) along six directions using a Bartington MS 2B laboratory sensor. The bulk magnetic susceptibility, χlf (measured in SI units), shows the magnetization acquired per unit field at low frequency. Anhysteretic remnant magnetization (ARM) was developed with peak alternating field of 100 mT in the presence of DC field 0.1 mT. χARM is obtained by dividing ARM by the strength of steady magnetic field (measured in SI unit). The isothermal remnant magnetism (IRM) was measured by an impulse magnetizer in both forward and backward fields 50, 100, 300, 500, 600, 800, 1000, 1200 mT and −10, −20, −30, −50, −100, −300, −400 mT, respectively (Kumar *et al.* 2017). The IRM_{1000} is referred to as the point of saturation isothermal remnant magnetism (SIRM). SIRM replicates the magnetic mineral concentration at fixed grain size. S_{ratio} was calculated by taking the negative ratio of IRM_{-300} and SIRM in order to constrain the relative concentration of high (hematite, goethite) or low (magnetite, maghemite) coercive minerals (Evans & Heller 2003; Basavaiah & Khadkikar, 2004).

4. Results

4.a. Sedimentology

The lithology of any given sample is based on the visual core description, microscopic observations from smear slides and other physical properties of the cored sediments. A composite lithology was constructed for Site U1457 using cores from Holes U1457A and U1457B (Pandey *et al.* 2016). Sediment at Site U1457 between 0 and 74 mbsf comprises a sequence of light-brown to light-greenish nannofossil oozes including foraminifer-rich nannofossil ooze and nannofossil-rich clay, interbedded with silty clay and silty sand dating from the Pleistocene to the Holocene. Hemiplegic sediments are represented by foraminifer-rich nannofossil ooze and nannofossil-rich clay. Sand–silt and clay-rich sediments are interbedded within the hemipelagic background and show sharp bases and normal grading. These latter sediments are interpreted as turbidites (Fig 2; Pandey *et al.* 2016).

4.b. Chronology and sedimentation rates

The age model of the core is based on the oxygen isotope stratigraphy reconstructed using 14 samples of planktic foraminifera from the uppermost ~40.8 m of the core. The chronology of the site was established by comparing the stable oxygen isotopic ratio of surface dwelling planktic foraminifer, *Globigerinoides ruber*, with the global isostack of Lisiecki & Raymo (2005) (Fig. 3a). A total of 15–20 clean specimens from 250–350 µm size fraction were picked for stable isotope measurement. The stable oxygen isotope analysis was carried out at Alfred Wegener Institute for Polar and Marine Research, Bremerhaven, Germany. In this study, five points were chosen from the top ~11.9 m core, covering the last ~217 ka (Fig. 3b).

4.c. Grain size

Grain-size characterization is a powerful proxy for understanding the depositional energy conditions and depositional processes. The particle sizes were characterized based on various standard statistical parameters, i.e. mean size, sorting, skewness and kurtosis. The mean size of the studied sediment ranges between 4.38 and 8 φ, which corresponds to a size range from very fine sand to clay. The sorting ranges from 1 to 1.85 φ, indicative of poorly sorted sediments (see Fig. 1s in the Supplementary Material available online at https://doi.org/10.1017/S0016756819000396). The studied core sediments have symmetric and fine to very fine negative skew at various depths, corresponding to depositional ages of 182–196, ~172, ~150.8, ~146, ~140.3 and ~63 ka; although negatively skewed sediments were also found at depths dated between 176 and ~190 ka. At these times, the mean size was an order of magnitude coarser and the concentration of coarse silt increased to ~30 % (Fig. 4).

The hydrological energy present during deposition is constrained by end-member modelling. In the water column, sediment is mixed by current activity, as well as biotic, terrestrial (detrital input) and chemical precipitation processes. Multimodal characteristics are acquired by the sediments through mixing during erosion, transportation and settling. EMMA is used to separate these detrital processes (Dietze *et al.* 2014). EMMA indicates the dominance of three end-members (see Fig. 2s A in the supplementary material available online at https://doi.org/10.1017/S0016756819000396): EM3, representing high-energy conditions dominated by coarse-silt and fine-sand size fractions; EM2, low-energy conditions dominated by fine and medium silt size particles; and EM1, lowest-energy conditions dominated by clay-sized particles. High proportions of EM3 suggest high-energy conditions, which could be due to high sediment flux from the continent from the contributing streams/rivers or simply the avulsion of the depositional lobe from one location to another on the fan surface. In contrast, high EM1 loadings indicate low-energy conditions and lower input from the continent, or sedimentation away from an active lobe. EM2 represents moderate hydrological conditions

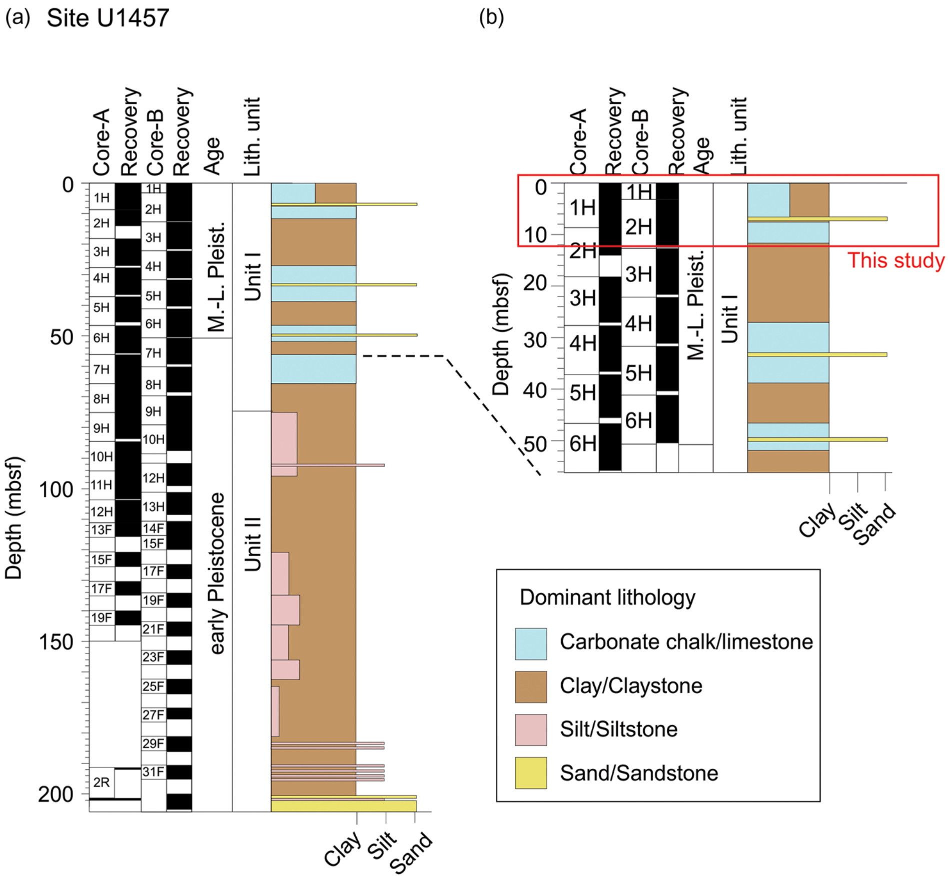

Fig. 2. (a) Detail lithostratigraphy of ~200 mbsf of Site U1457. (b) Schematic section of ~50 mbsf shows lithologic unit I with light-brown to light-greenish nannofossil ooze or foraminifer-rich nannofossil ooze, interbedded with silty sand and sandy silt, in addition to whitish calcareous ooze and clay enriched in carbonate and foraminifers as dominant lithology. The red rectangle shows present studied core depth 355-U1457-B2-H4-4-6.

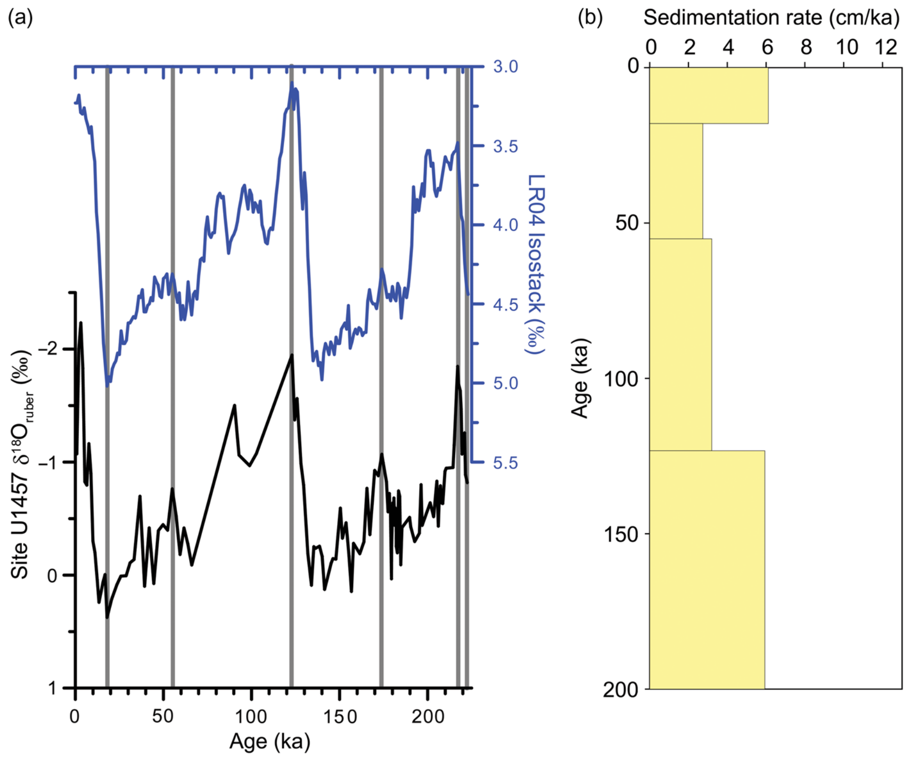

Fig. 3. (a) The chronology established by comparing the stable oxygen isotopic ratio of surface-dwelling planktic foraminifer, *Globigerinoides ruber*, with global isostack of Lisiecki & Raymo (2005). (b) Sedimentation rates at Site U1457.

https://doi.org/10.1017/S0016756819000396 Published online by Cambridge University Press

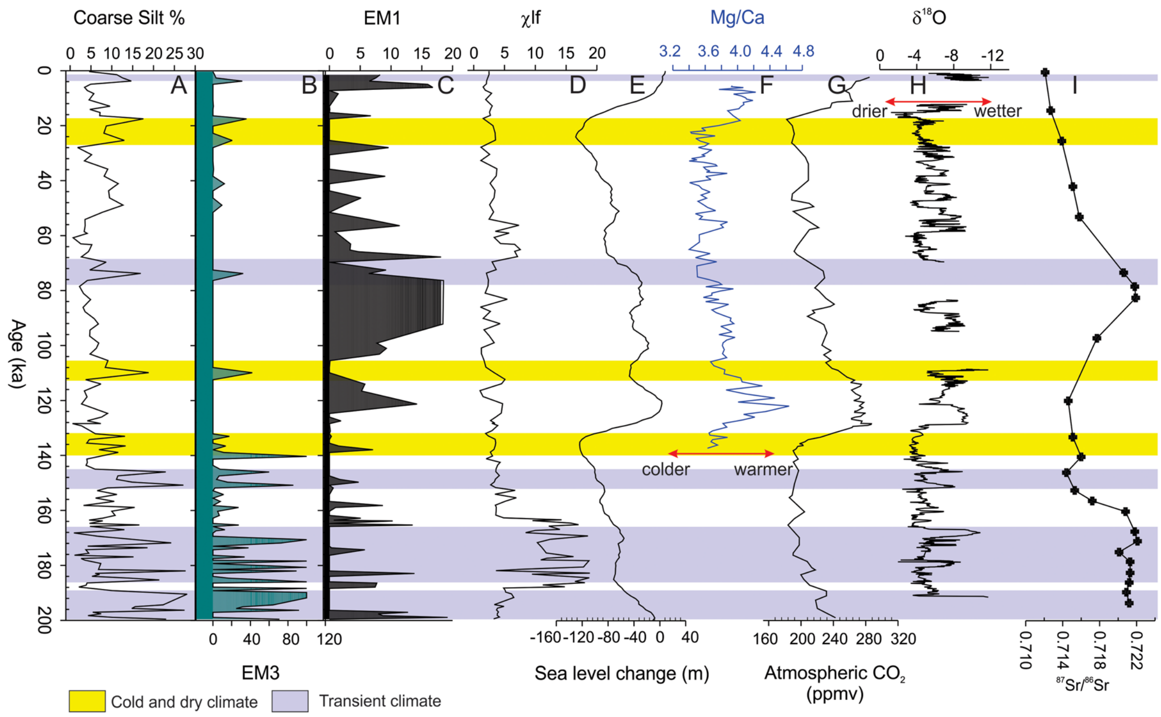

Fig. 4. (A) The coarse silt and (B) EM3 are used for high-energy conditions, (C) EM1 shows lowest-energy conditions and (D) χlf values from the Site 1457 Laxmi basin. This dataset is correlated with (E) the global sea-level fluctuation (Spratt & Lisiecki, 2016). (F) Blue line indicates sea surface temperature in the Arabian Sea reconstructed from Globigerina ruber (white) Mg/Ca ratio (Saraswat *et al.* 2005). (G) The global atmospheric CO_2 from Vostok ice core, Antarctica (Petit *et al.* 1999), (h) monsoon precipitation record from speleothem samples, Bittoo cave, NW India (Kathayat *et al.* 2016), and (I) detrital 87/86 isotopic ratio from Site U1456, Laxmi Basin, Arabian Sea, to delineate the source of the sediment (Khim *et al.* 2018). The purple bar represents the transient climate from the warmer to the cold, and the yellow bar cold climate and lowest sea level.

when both coarse and fine fractions were deposited, thus representing mixed sedimentation signals.

The average score of every end-member is measured over the whole of the grain-size distribution, and the contribution of end-members EM1, EM2, EM3 is 14.5, 43.4 and 42.0 %, respectively, which are measured with dominant modes 8.3, 6.6, 4.6 φ, respectively (see Fig. 2s B in the supplementary material available online at https://doi.org/10.1017/S0016756819000396). Although EM2 has the highest contribution, it cannot be used to decouple the hydrological processes.

Our results indicate a generally high but highly variable contribution of EM3 from 200 to 130 ka. Times of low EM3 values are accompanied by the high EM1 (Fig. 4). After 130 ka, the contribution of EM3 is low, while that of EM1 increased significantly. Some peaks indicating high contributions of EM3 are centred at 112, 74, 50, 44, 26, 18 and 4 ka. Coarse silt follows almost the same pattern as that of EM3. Highly variable coarse silt fraction was found in sediment dated from 200 to 130 ka, with an inconsistent increase and decrease up-section thereafter (Fig. 4).

4.d. Environmental magnetic parameters

The environmental magnetic properties are used to constrain the mineralogy and abundance of the magnetic grains and their composition from a mixed sediment with grains varying in size, shape and compositions. The bulk magnetic susceptibility of sediments is a proxy used to separate strong and weak remnant magnetization, i.e. ferromagnetic (magnetite, maghemite), antiferrimagnetic (hematite, goethite), paramagnetic (silicates, clays) and diamagnetic (quartz, carbonates) mineral grains (Liu *et al.* 2012). In marine sediments, magnetic parameters have been used to constrain the source of sediment, as well as the sediment transportation dynamics through enhancement in magnetic properties (Oldfield, 1991; Bloemendal *et al.* 1993; Evans & Heller, 2003). Figure 4 shows that magnetic susceptibility increased at ~188–160, ~152, ~116–108 and ~72–52 ka. The rapid increase in susceptibility corresponds to an increase in the concentration of magnetic grains in the coarser-grained sediment (coarse silt and mean grain size). The χlf and χARM, both depend upon the type of magnetic minerals in the bulk sediment (Bloemendal *et al.* 1993). A bivariate plot of χARM and χlf is used to understand the magnetic grain-size dependency (King *et al.* 1982). A regression line with confidence level of 95 % separates coarse and fine magnetic grains. Below the regression line the magnetic grains are coarser (5–7 φ), whereas above the line the size is ~1–4 φ (Fig. 5). The ratio of low to high coercive magnetic minerals is measured by estimating S_{ratio}. Values close to unity indicate the presence of the antiferromagnetic mineral magnetite at ~188–160 ka (see Fig. 3s in the supplementary material available online at https://doi.org/10.1017/S0016756819000396). The SIRM values suggest the presence of single, stable-domain magnetic grains. Bcr values are proportional to ferrimagnetic and antiferrimagnetic magnetic minerals, and therefore show the presence of few coercive minerals (magnetite and maghemite; see Fig. 3s in the supplementary material available online at https://doi.org/10.1017/S0016756819000396).

5. Discussion

Rivers play a major role in building marine stratigraphy by supplying sediment, but storage in terrestrial depocentres can buffer the sediment transport from source to sink (Goodbred, 2003). A complete sedimentary record is rarely preserved in continental basins

https://doi.org/10.1017/S0016756819000396 Published online by Cambridge University Press

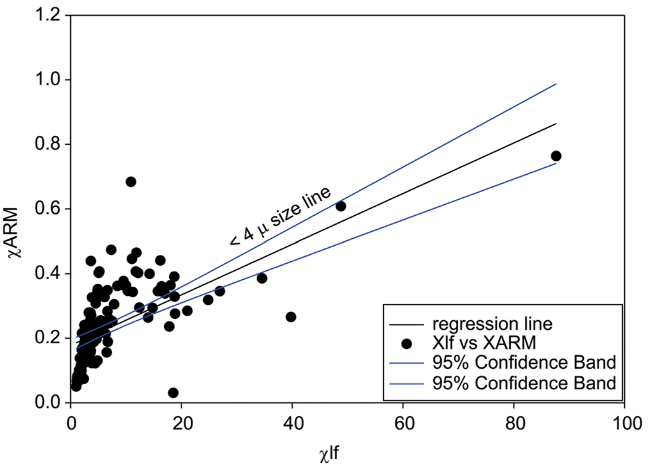

Fig. 5. A bivariate plot between χlf and χARM representing the grain-size control on the iron-bearing sediment (King's plot). The regression line (black line) and its zone within the 95 % confidence level (blue lines) shows the iron-bearing particle is <4µ.

because surface processes lead to erosion and generation of hiatuses, added to which age control can be difficult in the absence of fossils, which are typically more abundant in marine systems. Furthermore storage and reworking from terrestrial basins creates lags in sediment transportation downstream. In general the longer the transient zone in the sediment routing system, the greater the amount of sediment stored. The propagation of climate and/or tectonic signals through sediment transfer from source to sink depends upon the response time. The timing and magnitude of this mass storage can address the lags in propagation of sediment signal to downstream (Romans *et al.* 2016). Marine environments have more complete records than terrestrial equivalents that can be used to reconstruct the impacts of climate and environmental fluctuations, as well as the effects of tectonic perturbations, although these too are affected by upstream storage and recycling of older sediment (Clift & Giosan, 2014; Jonell *et al.* 2017). The present study involves physical properties such as grain size, EMMA and the environmental magnetic properties of the sediment from IODP Site U1457, representing the continental erosional input from the Indus and Narmada river systems. We now consider the erosional history in a series of temporal stages.

5.a. Sediment behaviour at ~200–130 ka

The high fluctuation in coarse silt concentration and EM3 content suggests significant instability in the hydrologic energy conditions during ~200–130 ka (Fig. 4). High χlf values are recorded, which indicate enhanced detrital flux to the proximal parts of the Indus Fan (drilling site) between 188 and 164 ka. The abrupt fluctuations in the coarse silt and EM3, as well as χlf, suggest a rapidly changing erosional flux, possibly linked to climatic conditions. Earlier studies indicate falling eustatic sea levels during this time; however, a slight rise is seen at ~170 and ~152–148 ka (Spratt & Lisiecki, 2016). Furthermore, a reduction in the atmospheric carbon dioxide (CO_2) and weak monsoon precipitation, as reconstructed from the speleothem record of Bittoo cave (NW India), characterize this period as a time of global cooling and weak summer monsoon (Petit *et al.* 1999; Kathayat *et al.* 2016). A significant cooling phase was also seen in the Indian Ocean sea surface temperatures (SSTs) reconstructed from the Mg/Ca values of planktonic foraminifer *Globigerinoides ruber* at ~137 ka (Saraswat *et al.* 2005).

These observations require an explanation as to why higher coarse silt and χlf are associated with a cold and dry climate during falling sea level and deteriorating climate. The large grain size and enhanced magnetic susceptibility indicate a dominance of terrestrial sediment over biogenic pelagic sediment. A large fraction of the sediment examined is detrital sediment fed by the Indus and/or the Narmada rivers. The enhanced coarse-grained sediment input could be explained by four possible processes: (i) erosion and sedimentation due to contemporaneous tectonic activities within the Laxmi Basin, (ii) tectonic activities driving faster erosion in the catchment area, (iii) faster sediment supply due to climate perturbations or a wetter, more erosive climate, and (iv) falling sea level. There is no known evidence for tectonic activities within the Laxmi Basin during the time of sedimentation. In any case, it would be very hard to decouple sedimentation in the deep ocean caused by erosion of older fan sediments from tectonically derived turbidity currents. Tectonic activities in the catchment area could lead to rapid river incision and therefore, an increase in coarser sediment supply. The lower Narmada River shows neotectonic evidence based on morphometric analysis, as well as deformation structures associated with entrenched meandering, and extensive, deep riverine formation during the late Quaternary (Chamyal *et al.* 2002; Joshi *et al.* 2013). More detailed work is needed to clearly attribute tectonic activities to high sediment transport to the Arabian Sea during ~200–130 ka. We consider past climate variability as another possibility. During cold and arid phases, Himalayan rivers reduced their discharge due to weakening in summer monsoon, despite the fact that the westerly precipitation helps to maintain a partly continuous flow, which in turn recycles sediment from the upper reaches of the river systems (Clift & Giosan, 2014; Jonell *et al.* 2017). The Indus and its tributaries carry sediment from the Himalaya and the Karakoram, where minerals like quartz and feldspars are relatively common. However, the Narmada River carries sediment mainly from the Deccan Trap basalt province. Sediments eroded from basalt are relatively high in iron-rich minerals and have high χlf, whereas Himalayan sediments have diluted magnetic signals and possess low χlf. We note that χlf is highest at 200–130 ka, and infer transportation from a source with high concentrations of iron-bearing minerals, possibly the Deccan Traps (i.e. sediment from the Narmada river system). The weakening of the Indian monsoon reduced the sediment flux from Indus and its tributaries, and hence caused a relative increase in sediment supply from the Narmada river system driving an enhancement in χlf. To further delineate the source of detritus and erosional hotspot in the catchment, $^{87}Sr/^{86}Sr$ and εNd isotopic compositions are estimated by Khim *et al.* (2018) and Yu *et al.* (2019). The isotopic composition values for $^{87}Sr/^{86}Sr$ and εNd from Sites U1457 and U1456 in the Laxmi Basin range from 0.7159 to 0.7255, −13.5 to −9.4, and 0.7121 to 0.7255, −12.5 to −8, respectively, since ~200 ka (Khim *et al.* 2018; Yu *et al.* 2019). Modern sediments of the Narmada and Indus rivers have overlapping isotopic ratios ($^{87}Sr/^{86}Sr$ and εNd for Indus and Narmada rivers are 0.722 and −13.5, and 0.721 and −11.9, respectively, within effective error (Jonell *et al.* 2018). Based on the $^{87}Sr/^{86}Sr$ and εNd isotopic composition, we suggest that the sediment at Site U1457 shows a mixed source from the Indus and Narmada basins. Our study, based on coarse-grained high-χlf sediment at Site U1457 (Fig. 4) supports an increased sediment load from the Narmada river system. The possibility of *in situ* iron precipitation is ignored here, because coarse-grained sediment is often transported (Fig. 5) (Maher, 2011).

Globally, sea level fell during ~200–130 ka (Spratt & Lisiecki, 2016), suggesting ice-volume increase in the northern hemisphere.

https://doi.org/10.1017/S0016756819000396 Published online by Cambridge University Press

The falling base level would have driven incision and an increase in the coarse silt fraction into the deep water. The augmentation in coarse silt and EM3 implies sediment transport by erosion of the delta and shelf areas, as well as the Indus canyon. Five erosive channels in the vicinity of Site U1457 (Mishra *et al.* 2016) and three major canyons along the middle Indus Fan margins imaged by a GLORIA side-scan sonar survey (Kolla & Coumes, 1987) have been identified. These canyons were perhaps active and may have transported the coarse silt towards Site U1457 between ~200 and 130 ka.

5.b. Sediment behaviour since 130 ka

Since ~130 ka, there have been several phases of intensification and weakening of the ISM (Clemens *et al.* 1991, 1996; Saraswat *et al.* 2005; Ziegler *et al.* 2010; Kathayat *et al.* 2016). During ~124–116, ~100–78, 60–52 and 30–28 ka, the clay-rich sediment shows high EM1 values (Fig. 4), which suggests that only the suspended load was transported to the drilling site, when the sea level was relatively high. At higher base level, only the finer fraction was transported to Site U1457, whereas the coarser fraction was stored in the apex or delta and/or middle fan area. The higher sea level is associated with intensification of the ISM and warmer climatic phases. At ~112–104 and ~25–18 ka we note enhanced coarse silt concentrations and higher EM3 values. At ~112–104 and ~25–18 ka, sea level fell ~40 and ~130 m (Lambeck & Chappell, 2001) compared to the present-day level, respectively. This implies that the sea-level change may drive terrigenous turbidite sedimentation in the Arabian Sea (Prins & Postma, 2000). At low sea level and high sediment flux, there were frequent turbidite events on the fan because of lack of buffering on the shelf and in the Indus Canyon. When coarse silt and EM3 were higher at ~78–68, 52–36 and ~4–2 ka, Bittoo cave and Guliya ice-core records suggest a transition in climate from warmer to colder (Thompson *et al.* 1997; Petit *et al.* 1999; Saraswat *et al.* 2005; Kathayat *et al.* 2016; Spratt & Lisiecki, 2016). Therefore, the higher EM3 associated with these periods can be explained as abrupt and short ISM phases. The eroded coarser sediment was transported and deposited to the drilling site as turbidites.

The $^{87}Sr/^{86}Sr$ and εNd values of sediment at Site U1456 at ~17 ka are 0.7127 and −8.3, respectively (Khim *et al.* 2018), which is similar to mean values of the Tapti River (0.7153 and −8.52) (Goswami *et al.* 2012). Therefore, the $^{87}Sr/^{86}Sr$ and εNd indicate that sediment deposited at ~17 ka was relatively more derived from the Tapti River, rather than the Indus.

The sea-level change controlled sedimentation on the Indus Fan (at sites Makran-469 and Indus-489) during ~12–11.5 ka, recorded by a significant decrease in turbidite sedimentation despite the fact that the sedimentation on the Makran continental slope was higher (Prins & Postma, 2000). Global fan building, e.g. the Amazon Fan, Mississippi Fan and Bengal Fan, occurred during transgression (Flood *et al.* 1991; Kolla & Perlmutter, 1993; Weber *et al.* 1997). The Mississippi Fan sediment recorded fan building and a spread of sediment into the deep ocean coupled with broadening of the sediment feeder catchment area during ice retreat (Fildani *et al.* 2016, 2018). High meltwater discharge and glacial lake outburst events dispersed enormous amounts of sediment to the Mississippi Fan during the late Pleistocene (Fildani *et al.* 2016, 2018). In contrast, the sedimentation rate in the eastern Arabian Sea (Indus Fan) was higher during regression while the transgression is associated with a cessation of sediment flux to the upper fan (Prins & Postma, 2000). These observations show that during falling sea level the increased sediment transport to the deeper part of the Indus Fan might be caused by an increase in fan gradient and canyon incision, as well as the elimination of storage space on the shelf. At the same time, the avulsion of fan lobes in the Laxmi Basin may have played a role in increasing the terrestrial sediment flux at the drill site. However, during sea-level rise, the coarser sediment is buffered in the nearshore zone and the shelf, with only fine-grained sediments reaching the coring site.

6. Conclusions

Abrupt fluctuations in the coarse silt and EM3 (sandy) grain-size fractions, as well as χlf, at IODP Site U1457 in the Laxmi Basin suggest rapidly changing erosion and sediment supply, possibly linked to climatic variability since ~200 ka. Sea level fell at ~200–130 ka (except at ~170 and ~148–152 ka), ~78–68 and 52–36 ka, accompanied by an increase in the coarse silt fraction. The higher coarse-silt and EM3 contents correlate with a time of regression, when there was an increase in the gradient due to base-level fall. This link between sea-level fall and increased grain size indicates that a fall in the base level of the Indus and Narmada river systems drives incision in the Indus delta, canyon and possibly even parts of the fan, leading to enhanced transfer of coarser sediment into deeper water. The consistent high χlf values of coarse sediment suggest preferential sediment transportation from the Deccan Traps (high in iron-bearing minerals) at these times.

In contrast, transgressive phases at ~124–116, ~100–78, ~60–52 and ~30–28 ka correlate with sedimentation of material with high EM1 during warm climatic phases with strong ISM. During these phases, the coarse sediments were deposited nearshore, close to the delta and on the flood plains of the lower reaches of the river so that only fine-grained sediments reached the coring site.

Author ORCIDs. Anil Kumar, 0000-0003-1559-8589, Rajeev Saraswat, 0000-0003-2110-2578, Peter D Clift, 0000-0001-6660-6388, Dhananjai Kumar Pandey, 0000-0001-6899-8995, Denise K Kulhanek, 0000-0002-2156-6383

Supplementary material. To view supplementary material for this article, please visit https://doi.org/10.1017/S0016756819000396.

Acknowledgements. IODP is gratefully acknowledged for providing the opportunity to work on board the vessel *JOIDES Resolution* during IODP Expedition 355 – Arabian Sea Monsoon. A.K. and S.D. thank the Director, Wadia Institute of Himalayan Geology (WIHG), for support and encouragement and allowing them to take up this project. A.K.G. thanks the DST, New Delhi, for a JC Bose fellowship. R.S. P.D.C. and Z.Y. appreciate the support from their respective heads. We thank Prof. A. Mackensen and the technical staff of the Alfred Wegener Institute for Polar and Marine Research, Germany, for the stable isotopic analysis. We also thank Dr Praveen K Mishra (WIHG) for helping us to understand the EMMA. Mr Jeet Majumdar (IIT Kharagpur) is also thanked for his help in data generation. The authors acknowledge IODP-India for the requisite support towards participation in IODP Expedition 355.

References

Basavaiah N and Khadkikar AS (2004) Environmental magnetism and its application towards palaeomonsoon reconstruction. *Journal of the Indian Geophysical Union* **8**, 1–14.

Bloemendal J, King JW, Hunt A, Demenocal PB and Hayashida A (1993) Origin of the sedimentary magnetic record at Ocean Drilling Program sites on the Owen Ridge, western Arabian Sea. *Journal of Geophysical Research: Solid Earth* **98**, 4199–5019.

Blum MD, Tomkin JH, Purcell A and Lancaster RR (2008) Ups and downs of the Mississippi Delta. *Geology* **36**, 675–78.

Burbank DW, Leland J, Fielding E, Anderson R, Brozovic N, Reid M and Duncan C (1996) Bedrock incision, rock uplift and threshold hillslopes in the northwestern Himalayas. *Nature* **379**, 505–10.
Cazenave A and Llovel W (2010) Contemporary sea level rise. *Annual Review of Marine Science* **2**, 145–73.
Chamyal LS, Maurya DM, Bhandari S and Raj R (2002) Late Quaternary geomorphic evolution of the lower Narmada valley, Western India: implications for neotectonic activity along the Narmada–Son Fault. *Geomorphology* **46**, 177–202.
Clemens SC, Murray DW and Prell WL (1996) Nonstationary phase of the Plio-Pleistocene Asian monsoon. *Science* **274**, 943–48
Clemens SC and Prell WL (1990) Late Pleistocene variability of Arabian Sea summer monsoon winds and continental aridity: Eolian records from the lithogenic component of deep-sea sediments. *Paleoceanography* **5**, 109–45.
Clemens S, Prell W, Murray D, Shimmield G and Weedon G (1991) Forcing mechanisms of the Indian Ocean monsoon. *Nature* **353**, 720.
Clift PD and Giosan L (2014) Sediment fluxes and buffering in the post-glacial Indus Basin. *Basin Research* **26**, 369–86.
Clift PD, Hodges KV, Heslop D, Hannigan R, Van Long H and Calves G (2008) Correlation of Himalayan exhumation rates and Asian monsoon intensity. *Nature Geoscience* **1**, 875–80.
Dietze E, Maussion F, Ahlborn M, Diekmann B, Hartmann K, Henkel K, Kasper T, Lockot G and Opitz S (2014) Sediment transport processes across the Tibetan Plateau inferred from robust grain size end-members in lake sediments. *Climate of the Past* **10**, 91–106.
Dutt S, Gupta AK, Wünnemann B and Yan D (2018) A long arid interlude in the Indian summer monsoon during ∼4,350 to 3,450 cal. Yr BP contemporaneous to displacement of the Indus valley civilization. *Quaternary International* **482**, 83–92.
Evans ME and Heller F (2003) *Environmental Magnetism: Principles and Applications of Environmental Magnetism.* Oxford: Academic Press.
Ferrier KL, Mitrovica JX, Giosan L and Clift PD (2015) Sea-level responses to erosion and deposition of sediment in the Indus River basin and the Arabian Sea. *Earth and Planetary Science Letters* **416**, 12–20.
Fildani A, McKay MP, Stockli D, Clark J, Dykstra ML, Stockli L and Hessler AM (2016) The ancestral Mississippi drainage archived in the late Wisconsin Mississippi deep-sea fan. *Geology* **44**, 479–82.
Fildani A, Hessler AM, Mason CC, McKay MP and Stockli DF (2018) Late Pleistocene glacial transitions in North America altered major river drainages, as revealed by deep-sea sediment. *Scientific reports* **8**, 13839.
Flood RD, Manley PL, Kowsmann RO, Appi CJ and Pirmez C (1991) Seismic facies and late Quaternary growth of Amazon submarine fan. In *Seismic Facies and Sedimentary Processes of Submarine Fans and Turbidite Systems* (eds P Weimer and MH Link), pp. 415–33. New York: Springer.
Goodbred SL, Jr (2003) Response of the Ganges dispersal system to climate change: a source-to-sink view since the last interstade. *Sedimentary Geology* **162**, 83–104.
Goswami V, Singh SK, Bhushan R and Rai VK (2012) Temporal variations in $^{87}Sr/^{86}Sr$ and εNd in sediments of the southeastern Arabian Sea: impact of monsoon and surface water circulation. *Geochemistry, Geophysics, Geosystems* **13**, Q01001, doi: 10.1029/2011GC003802.
Gupta AK, Anderson DM and Overpeck JT (2003) Abrupt changes in the Asian southwest monsoon during the Holocene and their links to the North Atlantic Ocean. *Nature* **421**, 354–7.
Gupta AK, Yuvaraja A, Prakasam M, Clemens SC and Velu A (2015) Evolution of the South Asian monsoon wind system since the late Middle Miocene. *Palaeogeography, Palaeoclimatology, Palaeoecology* **438**, 160–7.
Gupta H and Chakrapani GJ (2005) Temporal and spatial variations in water flow and sediment load in Narmada River Basin, India: natural and man-made factors. *Environmental Geology* **48**, 579–89.
Ivins ER, Dokka RK and Blom RG (2007) Post-glacial sediment load and subsidence in coastal Louisiana. *Geophysical Research Letters* **34**, L16303. doi: 10.1029/2007GL030003.
Jonell TN, Carter A, Böning P, Pahnke K and Clift PD (2017) Climatic and glacial impact on erosion patterns and sediment provenance in the Himalayan rain shadow, Zanskar River, NW India. *Geological Society of America Bulletin* **129**, 820–36, doi: 10.1130/B31573.
Jonell TN, Li Y, Blusztajn J, Giosan L and Clift PD (2018) Signal or noise? Isolating grain size effects on Nd and Sr isotope variability in Indus delta sediment provenance. *Chemical Geology* **485**, 56–73. doi: 10.1016/j.chemgeo.2018.03.036.
Joshi PN, Maurya DM and Chamyal LS (2013) Morphotectonic segmentation and spatial variability of neotectonic activity along the Narmada–Son Fault, Western India: remote sensing and GIS analysis. *Geomorphology* **180**, 292–306.
Kathayat G, Cheng H, Sinha A, Spötl C, Edwards RL, Zhang H, Li X, Yi L, Ning Y, Cai Y and Lui WL (2016) Indian monsoon variability on millennial-orbital timescales. *Scientific Reports* **6**, 24374. doi: 10.1038/srep24374.
Khim BK, Horikawa K, Asahara Y, Kim JE and Ikehara M (2018) Detrital Sr–Nd isotopes and sediment provenance in the Laxmi Basin of the Arabian Sea during the last 800 kyrs. *Geological Magazine*, 1–13. doi: 10.1017/S0016756818000596.
King J, Banerjee SK, Marvin J and Özdemir Ö (1982) A comparison of different magnetic methods for determining the relative grain size of magnetite in natural materials: some results from lake sediments. *Earth and Planetary Science Letters* **59**, 404–19.
Kolla V (2007) A review of sinuous channel avulsion patterns in some major deep-sea fans and factors controlling them. *Marine and Petroleum Geology* **24**, 450–69.
Kolla V and Coumes F (1987) Morphology, internal structure, seismic stratigraphy and sedimentation of the Indus Fan. *American Association of Petroleum Geologists Bulletin* **71**, 650–77.
Kolla V and Perlmutter MA (1993) Timing of turbidite sedimentation on the Mississippi Fan. *American Association of Petroleum Geologists Bulletin* **77**, 1129–41.
Kumar A and Srivastava P (2017) The role of climate and tectonics in aggradation and incision of the Indus River in the Ladakh Himalaya during the late Quaternary. *Quaternary Research* **87**, 363–85.
Kumar A, Srivastava P and Meena NK (2017) Late Pleistocene aeolian activity in the cold desert of Ladakh: a record from sand ramps. *Quaternary International* **443**, 13–28.
Lambeck K, and Chappell J (2001) Sea level change through the last glacial cycle. *Science* **292**, 679–86.
Li Y, Clift PD, Böning P, Blusztajn J, Murray RW, Ireland T, Pahnke K and Giosan L (2018) Continuous signal propagation in the Indus submarine canyon since the last deglacial. *Marine Geology*, **406**, 159–76. doi: 10.1016/j.margeo.2018.09.011.
Lisiecki LE and Raymo ME (2005) A Pliocene-Pleistocene stack of 57 globally distributed benthic $\delta^{18}O$ records. *Paleoceanography* **20**, PA1003. doi: 10.1029/2004PA001071.
Liu Q, Roberts AP, Larrasoana JC, Banerjee SK, Guyodo Y, Tauxe L and Oldfield F (2012) Environmental magnetism: principles and applications. *Reviews of Geophysics* **50**, RG4002. doi: 10.1024/2012RG000393.
Maher BA (2011) The magnetic properties of Quaternary aeolian dusts and sediments, and their palaeoclimatic significance. *Aeolian Research* **3**, 87–144.
Milliman JD and Syvitski JPM (1992) Geomorphic/tectonic control of sediment discharge to the ocean: the importance of small mountainous rivers. *The Journal of Geology* **100**, 525–44.
Mishra R, Pandey DK, Ramesh P and Clift PD (2016) Identification of new deep sea sinuous channels in the eastern Arabian Sea. *SpringerPlus* **5**, 844. doi: 10.1186/s40064-016-2497-6
Mitrovica JX and Milne GA (2002) On the origin of late Holocene sea-level highstands within equatorial ocean basins. *Quaternary Science Reviews* **21**, 2179–90.
Mitrovica JX, Tamisiea ME, Davis JL and Milne GA (2001) Recent mass balance of polar ice sheets inferred from patterns of global sea-level change. *Nature* **409**, 1026–9.
Munack H, Korup O, Resentini A, Limonta M, Garzanti E, Blöthe JH, Scherler D, Wittmann H and Kubik PW (2014) Postglacial denudation of western Tibetan Plateau margin outpaced by long-term exhumation. *Geological Society of America Bulletin* **126**, 1580–94.
Najman Y (2006) The detrital record of orogenesis: a review of approaches and techniques used in the Himalayan sedimentary basins. *Earth-Science Reviews* **74**, 1–72.

Oldfield F (1991) Environmental magnetism – a personal perspective. *Quaternary Science Reviews* **10**, 73–85.

Pandey DK, Clift PD, Kulhanek DK, Andò S, Bendle JAP, Bratenkov S, Griffith EM, Gurumurthy GP, Hahn A, Iwai M, Khim B-K, Kumar A, Kumar AG, Liddy HM, Lu H, Lyle MW, Mishra R, Radhakrishna T, Routledge CM, Saraswat R, Saxena R, Scardia G, Sharma GK, Singh AD, Steinke S, Suzuki K, Tauxe L, Tiwari M, Xu Z and Yu Z (2015) Expedition 355 Preliminary Report: Arabian Sea Monsoon. *International Ocean Discovery Program*. doi:10.14379/iodp.pr.355.2015

Pandey DK, Clift PD, Kulhanek DK, Andò S, Bendle JAP, Bratenkov S, Griffith EM, Gurumurthy GP, Hahn A, Iwai M, Khim B-K, Kumar A, Kumar AG, Liddy HM, Lu H, Lyle MW, Mishra R, Radhakrishna T, Routledge CM, Saraswat R, Saxena R, Scardia G, Sharma GK, Singh AD, Steinke S, Suzuki K, Tauxe L, Tiwari M, Xu Z and Yu Z (2016) Expedition 355 summary. In *Proceedings of the International Ocean Discovery Program, 355* (eds DK Pandey, PD Clift, DK Kulhanek and the Expedition 355 Scientists, Arabian Sea Monsoon). College Station, Texas: International Ocean Discovery Program.

Pandey A and Pandey DK (2015) Mechanism of crustal extension in the Laxmi Basin, Arabian Sea. *Geodesy and Geodynamics* **6**, 409–22.

Petit JR, Jouzel J, Raynaud D, Barkov NI, Barnola JM, Basile I, Bender M, Chappellaz J, Davis M, Delaygue G and Delmotte M (1999) Climate and atmospheric history of the past 420,000 years from the Vostok ice core, Antarctica. *Nature* **399**, 429–36.

Prerna R, Pandey D and Mishra R (2015) Approximation of flow patterns for submarine channel systems in the Arabian Sea using a GIS approach. *International Journal of Advanced Remote Sensing and GIS* **4,** 1142–60.

Prins MA and Postma G (2000) Effects of climate, sea level, and tectonics unraveled for last deglaciation turbidite records of the Arabian Sea. *Geology* **28**, 375–8.

Prizomwala SP, Bhatt N and Basavaiah N (2014) Provenance discrimination and source-to-sink studies from a dryland fluvial regime: an example from Kachchh, western India. *International Journal of Sediment Research* **29**, 99–109.

Romans BW, Castelltort S, Covault JA, Fildani A and Walsh JP (2016) Environmental signal propagation in sedimentary systems across timescales. *Earth-Science Reviews* **153**, 7–29.

Royer J-Y, Chaubey AK, Dyment J, Bhattacharya GC, Srinivas K, Yatheesh V and Ramprasad T (2002) Paleogene plate tectonic evolution of the Arabian and eastern Somali basins. In *The Tectonic and Climatic Evolution of the Arabian Sea Region* (eds PD Clift, D Kroon, C Gaedicke and J Craig), pp. 7–23. Geological Society of London, Special Publication no. 195(1).

Saraswat R, Nigam R, Weldeab S, Mackensen A and Naidu PD (2005). A first look at past sea surface temperatures in the equatorial Indian Ocean from Mg/Ca in foraminifera. *Geophysical Research Letters* **32**, L24605. doi: 10.1029/2005GL024093.

Simms AR, Anderson JB, Dewitt R, Lambeck K and Purcell A (2013) Quantifying rates of coastal subsidence since the last interglacial and the role of sediment loading. *Global and Planetary Change* **111**, 296–308.

Simms AR, Lambeck K, Purcell A, Anderson JB and Rodriguez AB (2007) Sea-level history of the Gulf of Mexico since the Last Glacial Maximum with implications for the melting history of the Laurentide Ice Sheet. *Quaternary Science Reviews* **26**, 920–40.

Spratt RM and Lisiecki LE (2016) A Late Pleistocene sea level stack. *Climate of the Past* **12**, 1079–92.

Thompson LG, Yao T, Davis ME, Henderson KA, Mosley-Thompson E, Lin PN, Beer J, Synal HA, Cole-Dai J and Bolzan JF (1997) Tropical climate instability: the Last Glacial Cycle from a Qinghai-Tibetan ice core. *Science* **276**, 1821–5.

Tripathi S, Tiwari M, Lee J, Khim BK, IODP Expedition 355 Scientists, Pandey DK, Clift PD, Kulhanek DK, Andò S, Bendle JA and Aharonovich S (2017) First evidence of denitrification vis-à-vis monsoon in the Arabian Sea since Late Miocene. *Scientific Reports* **7**, 43056.

Udden JA (1914) Mechanical composition of clastic sediments. *Bulletin of the Geological Society of America* **25**, 655–744.

Weber ME, Wiedicke MH, Kudrass HR, Hübscher C and Erlenkeuser H (1997) Active growth of the Bengal Fan during sea-level rise and highstand. *Geology* **25**, 315–18.

Weltje GJ and Prins MA (2003) Muddled or mixed? Inferring palaeoclimate from size distributions of deep-sea clastics. *Sedimentary Geology* **162**, 39–62.

Weltje GJ and Prins MA (2007) Genetically meaningful decomposition of grain-size distributions. *Sedimentary Geology* **202**, 409–24.

Wentworth CK (1922) A scale of grade and class terms for clastic sediments. *The Journal of Geology* **30**, 377–92.

Wolstencroft M, Shen Z, Törnqvist TE, Milne GA and Kulp M (2014) Understanding subsidence in the Mississippi Delta region due to sediment, ice, and ocean loading: insights from geophysical modeling. *Journal of Geophysical Research: Solid Earth* **119**, 3838–56.

Yu Z, Colin C, Wan S, Saraswat R, Song L, Xu Z, Clift P, Lu H, Lyle M, Kulhanek D, Hahn A, Tiwari M, Mishra R, Miska S and Kumar A (2019) Sea level-controlled sediment transport to the eastern Arabian Sea over the past 600 kyr: clay minerals and Sr-Nd isotopic evidence from IODP site U1457. *Quaternary Science Reviews* **205**, 22–34.

Ziegler M, Lourens LJ, Tuenter E and Reichart GJ (2010) High Arabian Sea productivity conditions during MIS 13 – odd monsoon event or intensified overturning circulation at the end of the Mid-Pleistocene transition? *Climate of the Past* **6**, 63–76.